SAND-77-0478C

CONF-770642--1

CHANNELING ANALYSIS OF STACKING DEFECTS IN EPITAXIAL Si LAYERS

S. U. Campisano, G. Foti, E. Rimini
Istituto di Struttura deall Materia, Universita di Catania
Corso Italia, 57 - I95129 Catania, Italy

S. T. Picraux*
Sandia Laboratories, Albuquerque, New Mexico 87115

The channeling effect technique has been applied to investigate dechanneling by stacking defects in heteroepitaxially grown silicon. Ion backscattering was performed on 0.9 μm Si layers grown on sapphire as a function of beam energy (1.1 to 2.5 MeV He^+), projectile ion (He^+, D^+) and crystal direction (<100>,<111>,<112>, <113>). Transmission electron microscopy analysis reavealed the presence of a high density of stacking faults and twin lamellae. A model based on the new interior surfaces presented by such stacking defects is used to calculate the dechanneling cross section, and the disorder profiles are obtained from the experimental dechanneled fractions in terms of displaced rows per unit volume. Direct backscattering of channeled particles from the defects is neglected since the dechanneling cross section per row is about one order of magnitude larger than that per displaced atom. The resulting defect depth distributions are independent of beam energy and projectile ion, and give improved quantitative agreement with previous studies. The application of channeling to stacking-defect measurements requires a minimum density of ~ 10^{15} displaced rows/cm^2.

*Supported in part by the U. S. Energy Research and Development Administration, under Contract AT(29-1)789.

DISCLAIMER

INTRODUCTION

The channeling technique, in combination with ion backscattering, has been widely used to investigate damage in ion implanted semiconductors. The power of this technique resides mainly in the ability to determine the depth distribution of damage. In a quantitative analysis one must determine or assume the type of damage present in order to utilize the appropriate dechanneling cross section. Often the nature of the damage can be determined by other techniques, such as electron microscopy. A simple type of disorder in terms of the dechanneling calculation is that of small isolated regions of amorphous material. This is closely approximated by heavy ion implantation in the semiconductors Si and Ge as revealed by other structure sensitive techniques.[1]

Care has to be taken in order to use a correct dechanneling cross section in the extension of the channeling technique to the analysis of other defects like those induced by ion implantation in metals or growth processes in heteroepitaxial layers. For example, detailed measurements by ion channeling and transmission electron microscopy (TEM) have been carried out recently to characterize implanted Aℓ.[2,3] Dislocations were the dominant type of defect present and the incident ion type and energy dependences of the dechanneling cross section were used for a quantitative evaluation of the damage. From these studies an improved understanding of the quantitative analysis and the sensitivity limitations of the channeling

technique clearly emerge. Detailed considerations have also been given in the channeling analysis of implanted Au.[4]

For additional understanding of the channeling technique as a probe of defects, we consider improvements upon a previous analysis (5) of Si thin crystals grown heteroepitaxially on sapphire and spinel. TEM and etch pits have shown that these heteroepitaxial Si layers contain a large number of stacking defects including stacking faults and twin lamellae whose densities decrease from the interface to the film surface. The present measurements and analysis of heteroepitaxial Si layers have been carried out with the aim of detailing the dependence of the dechanneling, and then of the extracted defect profile, on experimental parameters such as crystallographic direction, atomic number and energy of the analyzing beam.

Results and Discussion

Single crystal Si layers grown epitaxially on sapphire were obtained from RCA and Union Carbide, with the majority of the measurements being made on layers 0.9 μm thick. TEM measurements on these samples showed high densities of stacking faults and twin lamellae consistent with previous studies. Figures 1a and 1b show representative micrographs of stacking faults in bright field and twin lamellae in dark field, respectively. The average thickness of the twin lamellae are determined to be $\approx$ 20 Å corresponding to $\approx$ 4 atoms per <111> row based on the streaking of the (111) twin diffraction spots for (110) matrix diffraction.

The influence of stacking faults on dechanneling can be visualized with the aid of Fig. 2. The stacking sequence of {111} planes in a perfect diamond-type lattice is Aa Bb Cc Aa Bb Cc. An intrinsic fault, characterized by the missing plane Aa, changes the sequence to that shown in the lower left part of Fig. 2. Particles impinging along a direction parallel or normal to the fault plane, for both planar and axial channeling are not distrubed by the fault. Along other directions particles enter a perfect lattice (full circles) and traversing the fault plane will still move in a perfect crystal (open circles) shifted with respect to that already traversed, as illustrated in Fig. 2 for the <100>,<110> and <111> directions. Twin lamellae also occur on {111} planes and the twinned material gives rise to a new set of rows in this case consisting of ~ 4 atoms each. In addition, after passing through both boundaries of a twin lamella, there are equal probabilities that the stacking sequence will have zero, one or two planes missing and this is equivalent to no fault, an intrinsic fault or an extrinsic fault, respectively. For the thin twin lamellae of these studies the contribution from the volume of the twins plus the 2/3's contribution after passing through the twin boundaries will on the average be essentially equivalent to that for a stacking fault within the accuracies of the present analysis. Thus both of these types of stacking defects introduce new crystal surfaces to the channeled ions.

As a first approximation the dechanneling due to a stacking fault can be related to the minimum yield for a beam entering

a crystal parallel to a low index axis or plane. In this description the dechanneling probability per row is given by

$$\sigma_{row} = \frac{\chi_o}{Nd} \quad , \tag{1}$$

where χ_o is the surface yield of a perfect crystal of atomic density N and d is the spacing along the row.

In contrast, the dechanneling by a displaced atom can be estimated on the basis of the Rutherford cross section, giving:[7]

$$\sigma_{atom} = \frac{\pi Z_1^2 Z_2^2 e^4}{E^2 \psi_{1/2}^2} \quad , \tag{2}$$

where Z_1 and Z_2 are the atomic numbers of projectile and target atoms, respectively, E the beam energy and $\psi_{1/2}$ the experimental critical angle for channeling. As a simple estimate, for 2.0 MeV He impinging along the <100> axis in Si at room temperature the dechanneling cross section due to a stacking fault, σ_{row}, is about one order of magnitude larget than σ_{atom}. This larger value of the dechanneling cross section allows us to neglect the direct contribution to the aligned yield in comparison with the dechanneling one.

In addition, the two dechanneling cross sections differ in their dependence on experimental parameters. We have observed the dependence of the dechanneling on the beam energy, the atomic number of the analyzing projectile and the crystallographic direction. The latter is also related to the structure of defects and to their distribution on the four equivalent {111} planes.

Experimental energy spectra for an He^+ beam of several energies impinging along the <100> axis of a ≈ 0.9 μm thick Si layer grown on sapphire are shown in Fig. 3. The aligned yields for all the beam energies are comparable near the surface to those of a perfect crystal and they increase, approaching a maximum at the interface with the substrate. The corresponding dechanneled fractions, i.e., the ratio of aligned-to-random yields, are shown in Fig. 4. The energy-to-depth conversion has been made assuming bulk density for random spectra and assuming a constant ratio for the aligned energy loss given by the experimental aligned-to-random energy-width ratio. The dechanneled fractions show a small energy dependence and they increase with decreasing beam energy. For comparison the dechanneled fractions for a <100> Si crystal are also shown in Fig. 4. A small energy dependence is evident for the Si crystal, in agreement with previous investigations of dechanneling in perfect crystals.[8]

For comparison with the energy dependence of dechanneling due to displaced atoms or small amorphous zones, a Si crystal has been implanted with 300 keV N^+ and analyzed with He^+ beams at different energies. The corresponding dechanneled fractions are shown in Fig. 5 and a much more pronounced energy dependence results just after the damaged region, with the dechanneling increasing with decreasing beam energy. These results point out, without detailed data analysis, that the energy dependence of the dechanneled fraction for the heteroepitaxial Si layers is negligible, in agreement with that predicted by σ_{row}. In

fact σ_{row} defined in Eq. 1 is given by

$$\sigma_{row} = \pi(2u_1^2 + a_{TF}^2) \quad , \tag{3}$$

or by

$$\sigma_{row} = 18.8u_1^2 \quad , \tag{4}$$

where u is the rms unidimensional vibration amplitude and a_{TF} the Thomas-Fermi screening distance. Eqs. 3 and 4 are obtained from the continuum approximation[9] and from an empirical fit, respectively.[10]

The same epitaxial layers have been analyzed along different crystallographic directions and the resulting dechanneled fractions are shown in Fig. 6. Neglecting the direct backscattering from the extra planes, in accordance with our estimates, the random component of the beam coincides with the aligned yield and is given by:

$$\chi_D(z) = \chi_v(z) + (1 - \chi_v(z))\ P(q_D) \quad , \tag{5}$$

where $\chi_v(z)$ is the dechanneled fraction in the virgin crystal measured at the depth z and $P(q_D)$ represents the probability that a beam of intensity $(1 - \chi_D(z))$, having initially a δ-function distribution is dechanneled after traversing a number q_D of displaced rows/cm^2. The value $P(q_D)$ can be estimated following the Bøgh[7] approach and it is given by

$$P(q_D) = 1 - \exp\left[-\sigma_{row}\int_0^Z N_{row}(z)\, dz\right] \quad , \tag{6}$$

where $q_D = \int_0^Z N_{row}(z)dz$ and $N_{row}(z)$ represents the number of displaced rows/cm^3. From Eqs. 5 and 6 we obtain

$$\frac{1 - \chi_D(z)}{1 - \chi_v(z)} = \exp\left[-\sigma_{row} \cdot q_D(z)\right] \quad . \tag{7}$$

The experimental $\frac{1 - \chi_D(z)}{1 - \chi_v(z)}$ values are plotted on a semilog scale in Fig. 7a for different energies of the analyzing He^+ beam and in 7b for several channeling directions. The resulting integral defect profile in Fig. 7a is energy independent, thus confirming that σ_{row} is energy independent too, in agreement with our model. In addition, analysis of 1.0 MeV deuterium spectra for the <100> axis gives results which nearly coincide with that obtained using a helium analysis beam. For the different crystal directions in Fig. 7b a difference of about 10-20% is seen, but this is too small to conclude a spatial order in the arrangement of the stacking defects. Thus, they are considered to be randomly distributed on the four available $\{111\}$ planes.

The fast decrease of the $\frac{1 - \chi_D(z)}{1 - \chi_v(z)}$ values near the interface with the substrate is related to the large number of defects present in this region. In the same plot several straight lines are drawn corresponding to different uniform distributions of displaced rows. The numbers are obtained using the empirical fit value (Eq. 4) for the dechanneling cross section. The lines intersect the experimental values at different depths,

and for each of these the integrated number of N_{row} traversed by the analyzing beam is equal to the N_{row} label of the corresponding line multiplied by the intersection depth.

The defect depth profiles obtained by the present method and by the standard approach[6] for damage analysis are compared in Fig. 8. The upper curve was obtained by the standard approach using the dechanneling cross section for Rutherford scattering from single atoms (Eq. 2) and including direct backscattering. The slopes of the profiles are almost equal and the two profiles differ by about one order of magnitude. This difference between the two profiles is due to the difference in the dechanneling cross section for displaced atoms and rows, respectively. Note that the upper curve gives the profile in terms of displaced atoms per cm^3 while the lower one provides the displaced rows per cm^3. This improved dechanneling analysis is in agreement with previous quantitative studies of heteroepitaxial Si which gave densities of scattering centers by the standard analysis a factor of 10-70 over the number of displaced rows as determined by etch line counting and layer removal techniques.[6]

From the present work we conclude that a stacking defect density corresponding to ~ 10^{15} displaced rows/cm^2 is required for detection by single-alignment channeling. This corresponds to approximately one atomic plane (≈ 2.5 x 10^{15}/cm^2 for <100> Si) and would give rise

to an increase in the channeling yield of ~ 3%. In contrast, this lower limit for channeling analysis represents an approximate upper limit for quantitative TEM analysis, since an effective areal coverage greater than one monolayer will result in appreciable defect image overlap.

Acknowledgements: Transmission electron microscopy measurements by C. R. Hills and discussions with T. J. Headley are gratefully acknowledged.

REFERENCES

1. J. W. Mayer, L. Eriksson and J. A. Davies, "Ion Implantation in Semiconductors," (Academic Press, NY, 1970) Chap 3 and references quoted therein.
2. G. Foti, S. T. Picraux, S. U. Campisano, E. Rimini and R. A. Kant, "Dechanneling by Dislocations in Zn-implanted Al," Proceedings of the Fifth International Conference on Ion Implantation, Ed. by F. Chernow, D. K. Brice and J. A. Borders (Plenum Press, NY, 1977) in press.
3. S. T. Picraux, E. Rimini, G. Foti and S. U. Campisano (to be published).
4. P. P. Pronko, Nucl. Inst. and Methods 132, (1976) 249.
5. S. T. Picraux, J. Appl. Phys. 44, (1973) 587.
6. S. T. Picraux and G. J. Thomas, J. Appl. Phys. 44, (1973) 594.
7. E. Bøgh, Can. J. Phys. 46, (1968) 653.
8. B. T. Appleton and G. Foti "Channeling," in Ion Beam Material Analysis, ed. by J. W. Mayer and E. Rimini (Academic Press, NY, 1977) in press.
9. L. Lindhard, K. Dan. Vidensk. Selsk. Mat-Fys. Medd. 34, (1965) n. 14.
10. J. H. Barret, Phys. Rev. 3B, (1971) 1527.

FIGURE CAPTIONS

Fig. 1 TEM micrographs of Si grown on sapphire showing (a) stacking faults and (b) dark field image of twin lamellae with a (114) matrix and corresponding (110) twin diffraction pattern shown in the inset.

Fig. 2 Schematic illustration of the stacking sequence in the presence of a fault in the Si lattice where along the <100>,<111> and <110> directions two perfect lattices (●) and (○) are seen shifted with respect to each other.

Fig. 3 Random and <100> energy spectra of 1.13, 2.0 and 2.5 MeV He^+ ions scattered at 165° from a ≈ 0.9 μm thick Si crystal grown on sapphire.

Fig. 4 Ratio of aligned to random yield as a function of the depth for data of Fig. 3 and for a bulk <100> Si crystal.

Fig. 5 Ratio aligned to random yield vs. depth for a Si <111> crystal damaged with 200 keV N^+ ions and analyzed with 1.0, 1.5 and 2.5 MeV He^+.

Fig. 6 Ratio of aligned to random yield for the indicated axes vs. depth of 2.0 MeV He^+ ions for bulk <100> Si and for a ~ 0.9 μm thick Si crystal grown on sapphire.

Fig. 7 Integral distributions of displaced rows vs. depth in the epitaxial Si crystal a) for different He^+ beam energies and b) for the 2.0 MeV He beam along

several crystal directions. Straight lines correspond to uniform distributions of displaced rows for the densities indicated.

Fig. 8 Comparison between the differential defect profiles obtained by the present approach and the "standard" one using the Rutherford cross section. The scale is in atom/cm^3 for the standard approach and in rows/cm^3 for the present treatment.

THIS PAGE

WAS INTENTIONALLY

LEFT BLANK

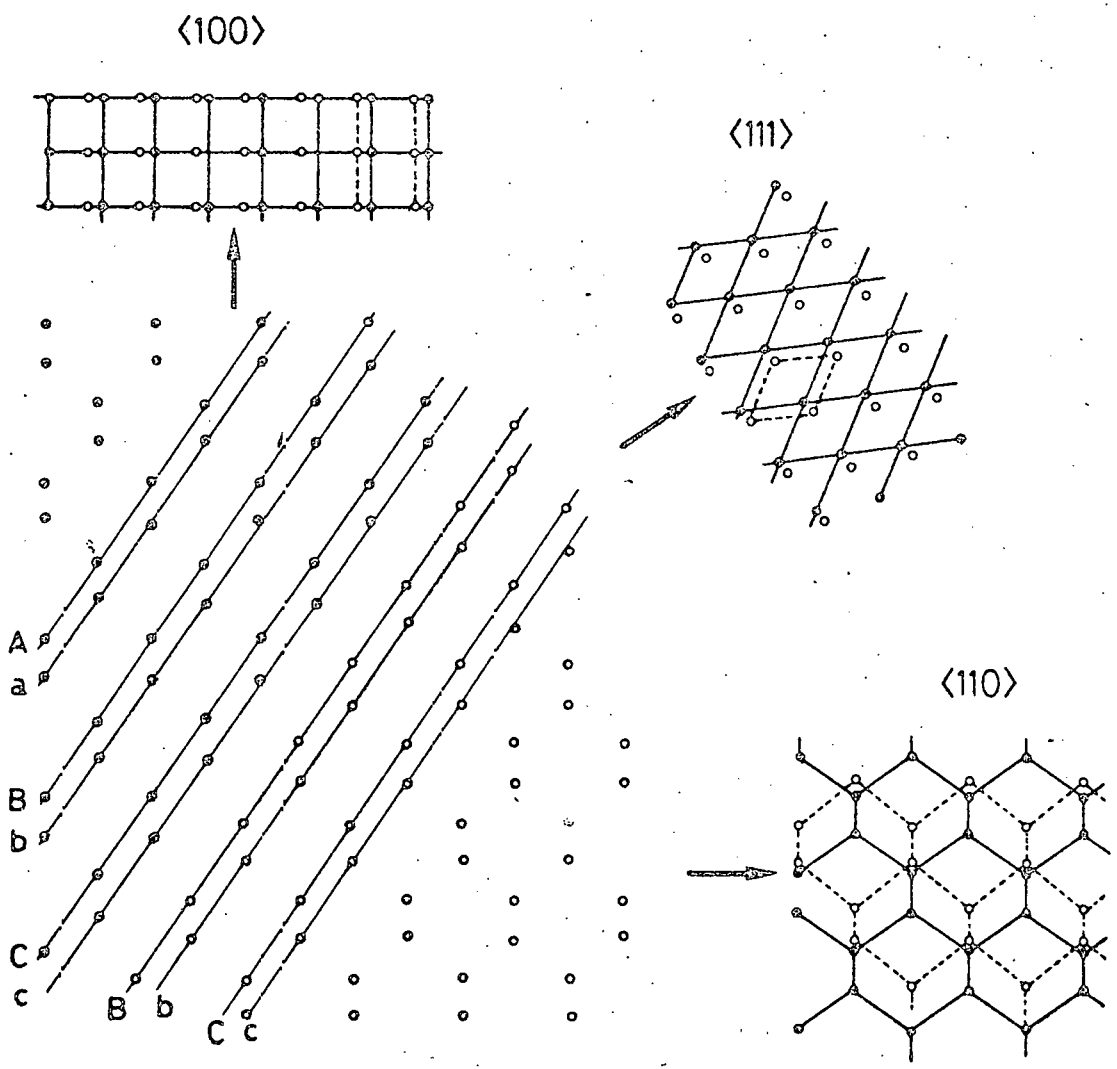

Intrinsic Stacking Fault in the Si Lattice

Fig 2

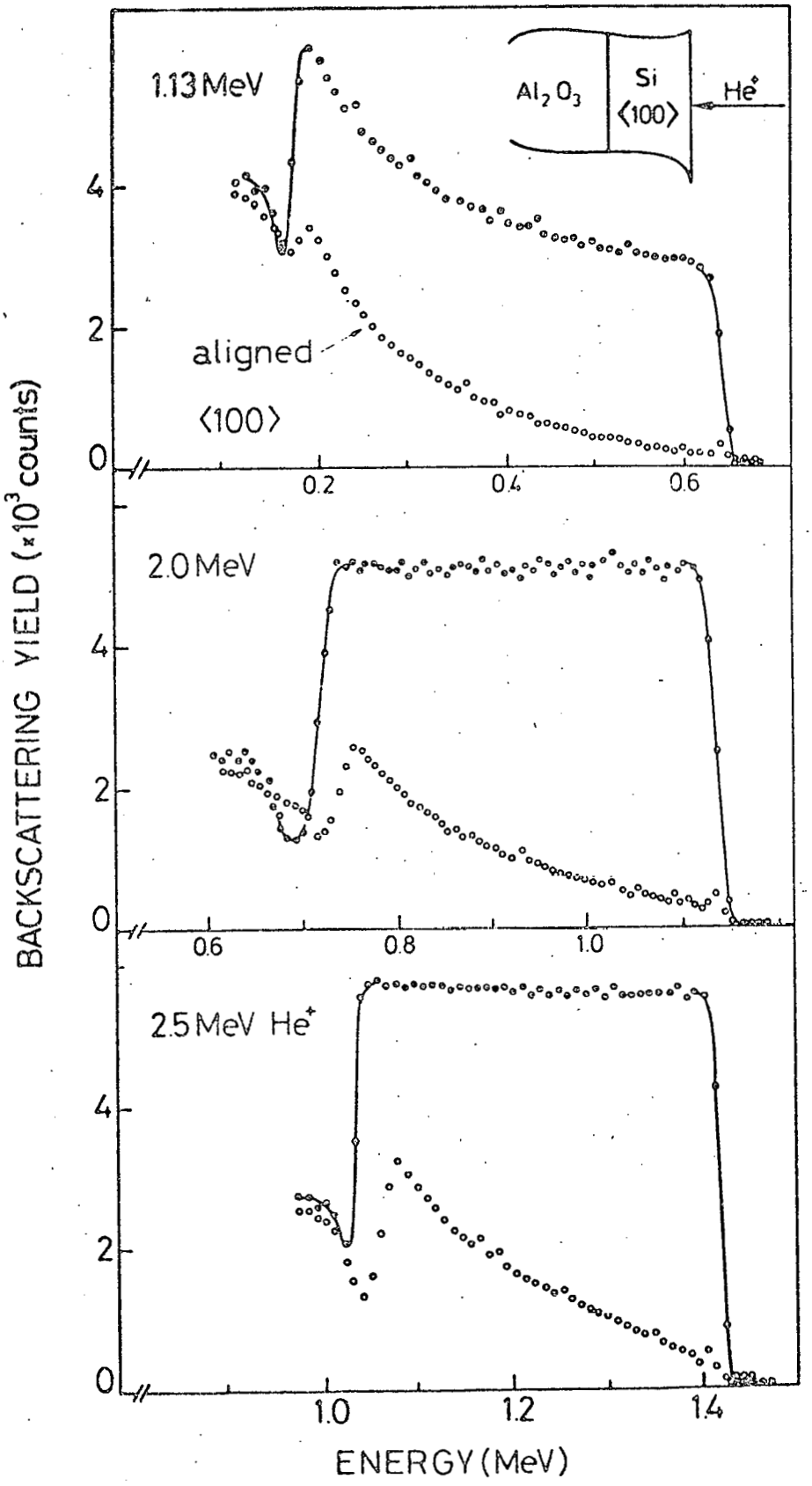
1.13 MeV
Al_2O_3
Si
⟨100⟩
He⁺
aligned
⟨100⟩
2.0 MeV
2.5 MeV He⁺
BACKSCATTERING YIELD (×10³ counts)
ENERGY (MeV)
0
2
4
0.2
0.4
0.6
0.8
1.0
1.2
1.4

Fig 3

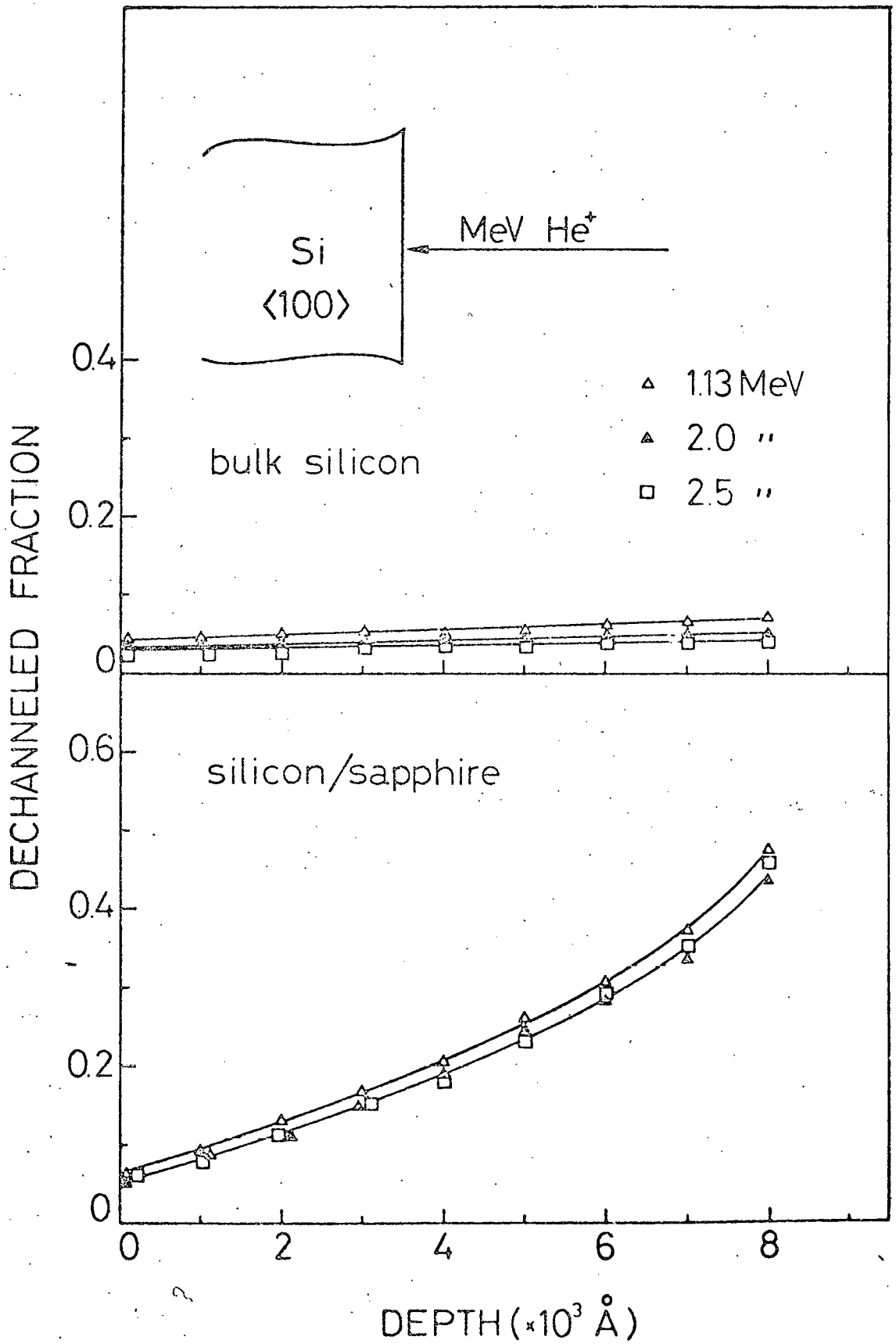
Si
⟨100⟩
MeV He+
1.13 MeV
2.0 "
2.5 "
bulk silicon
silicon/sapphire
DECHANNELED FRACTION
DEPTH (×10³ Å)
0
0.2
0.4
0.6
2
4
6
8

Fig. 4

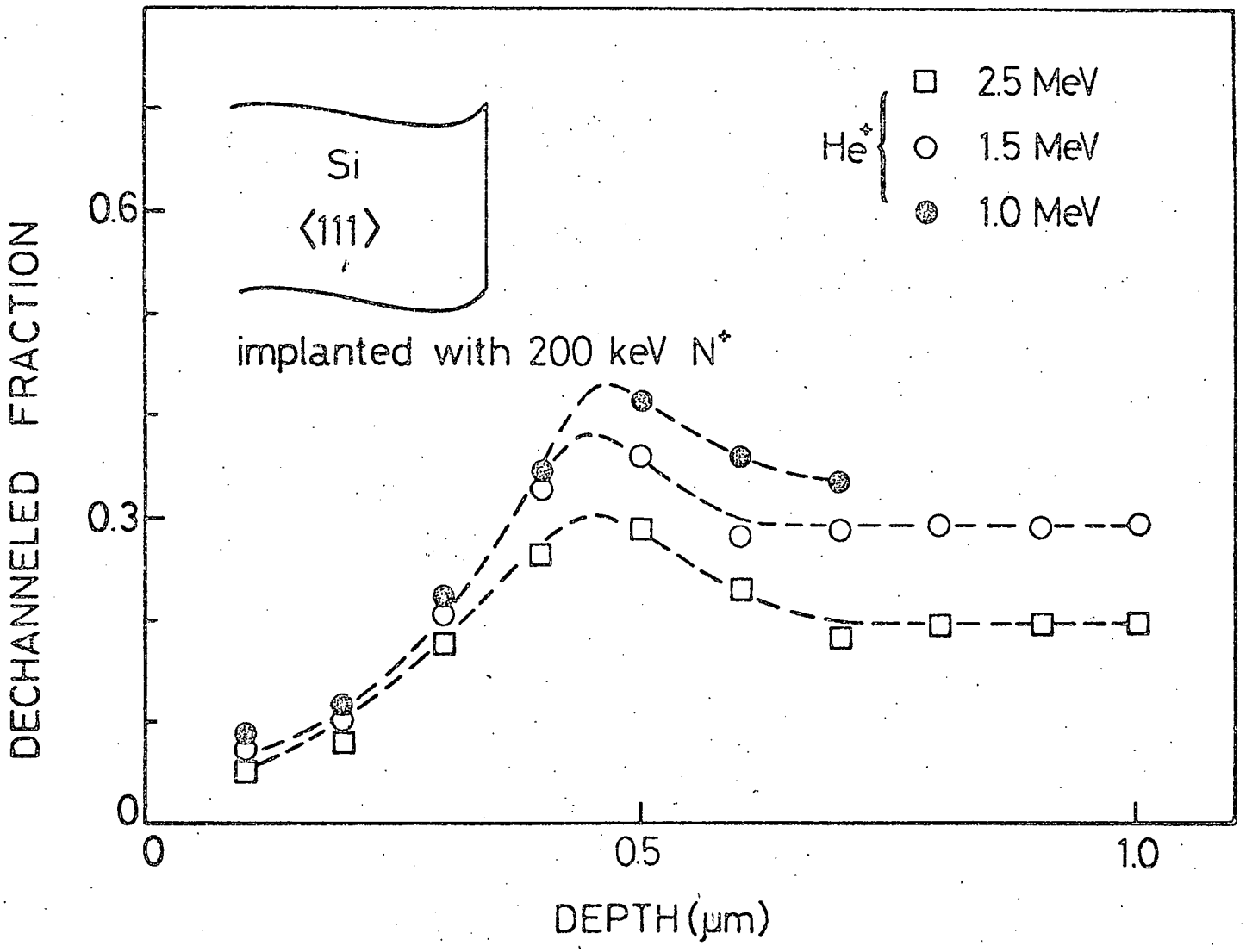
Si
⟨111⟩
implanted with 200 keV N+
He+
2.5 MeV
1.5 MeV
1.0 MeV
DECHANNELED FRACTION
0.6
0.3
0
0
0.5
1.0
DEPTH (μm)

Fig 5

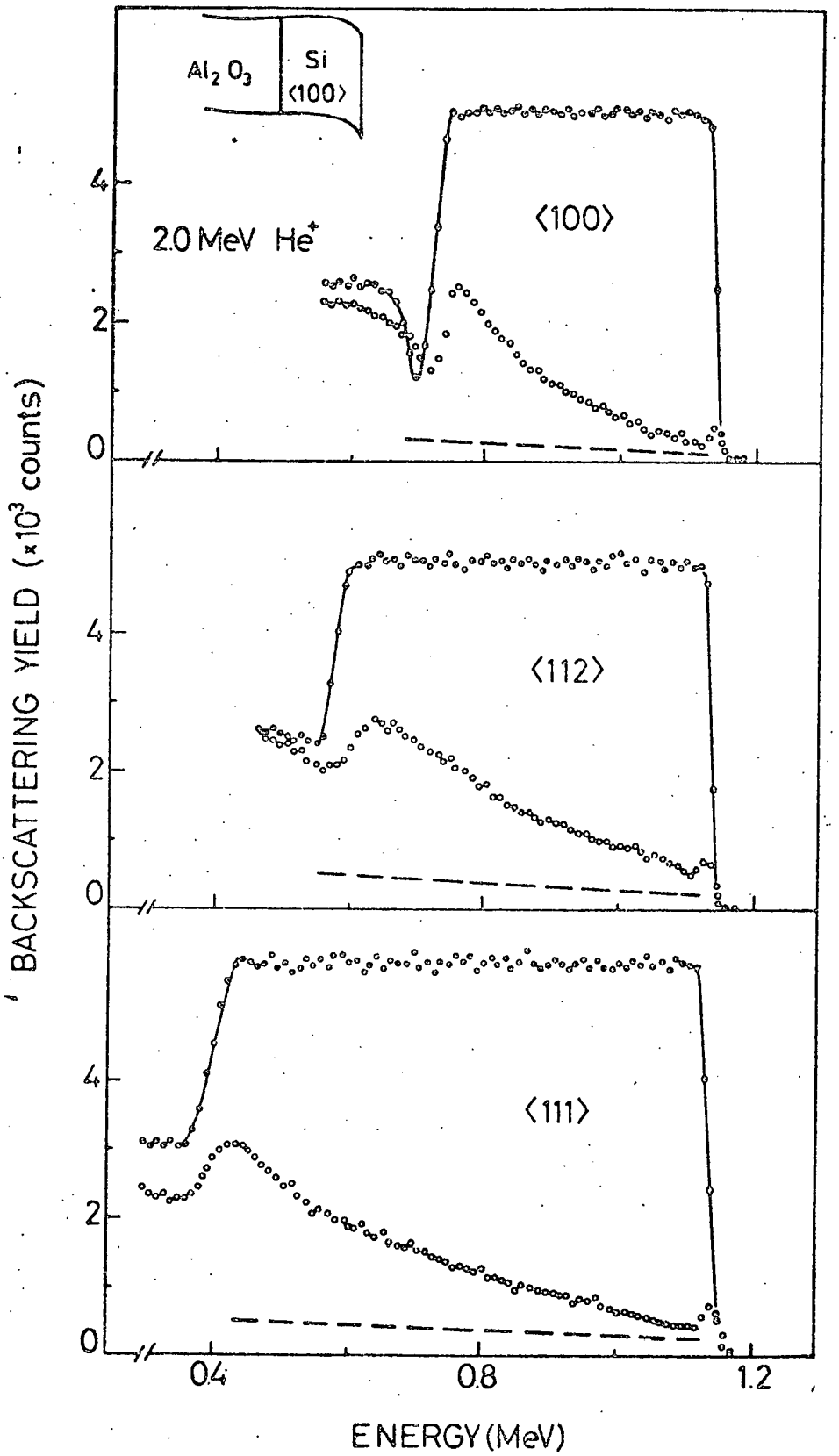
Al2 O3
Si
⟨100⟩
2.0 MeV He+
⟨100⟩
⟨112⟩
⟨111⟩
BACKSCATTERING YIELD (×10³ counts)
ENERGY (MeV)
0
2
4
0.4
0.8
1.2

Fig 6

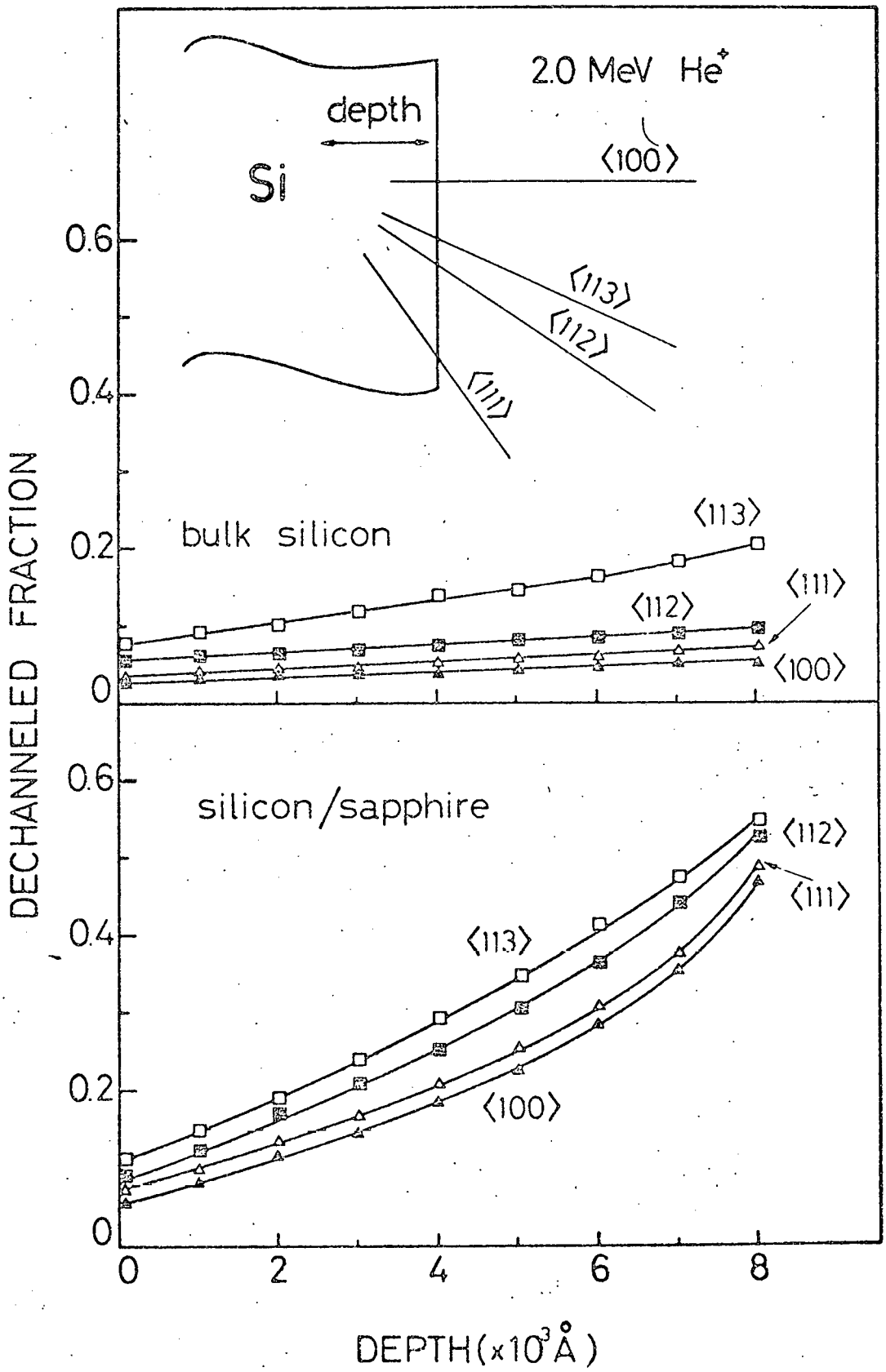
2.0 MeV He+
depth
Si
⟨100⟩
⟨113⟩
⟨112⟩
⟨111⟩
bulk silicon
silicon/sapphire
DECHANNELED FRACTION
DEPTH(×10³Å)
0
0.2
0.4
0.6
2
4
6
8

Fig 7

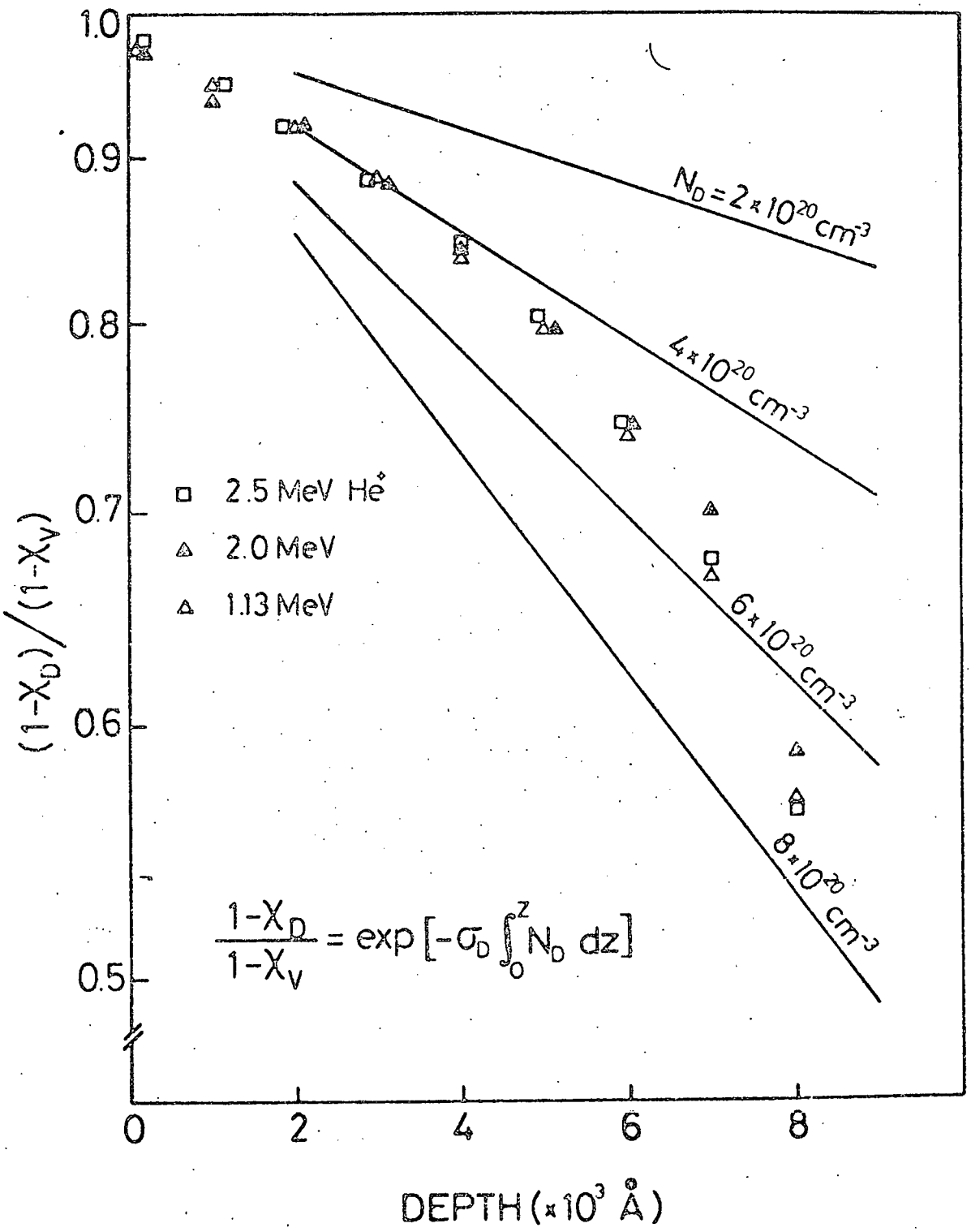
1.0
0.9
0.8
0.7
0.6
0.5
0
2
4
6
8
$(1-X_D)/(1-X_V)$
DEPTH ($\times 10^3$ Å)
$N_D = 2 \times 10^{20}$ cm^{-3}
4×10^{20} cm^{-3}
6×10^{20} cm^{-3}
8×10^{20} cm^{-3}
2.5 MeV He$^+$
2.0 MeV
1.13 MeV
$\frac{1-X_D}{1-X_V} = \exp\left[-\sigma_D \int_0^z N_D \, dz\right]$

Fig 8

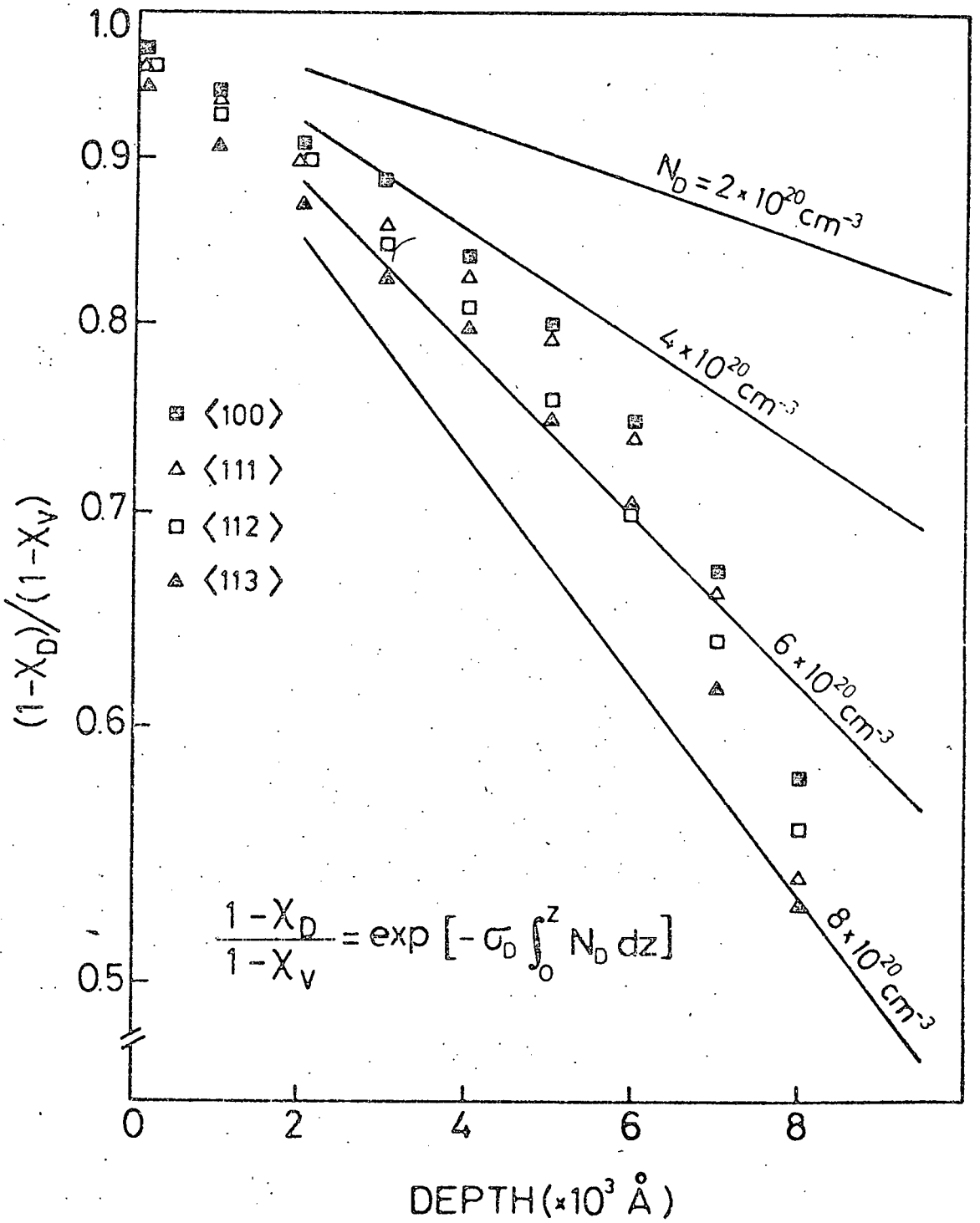
1.0
0.9
0.8
0.7
0.6
0.5
0
2
4
6
8
$(1-\chi_D)/(1-\chi_V)$
DEPTH ($\times 10^3$ Å)
$N_D = 2\times10^{20}\,cm^{-3}$
$4\times10^{20}\,cm^{-3}$
$6\times10^{20}\,cm^{-3}$
$8\times10^{20}\,cm^{-3}$
⟨100⟩
⟨111⟩
⟨112⟩
⟨113⟩
$\frac{1-\chi_D}{1-\chi_V} = \exp\left[-\sigma_D \int_0^z N_D\, dz\right]$

Fig 9

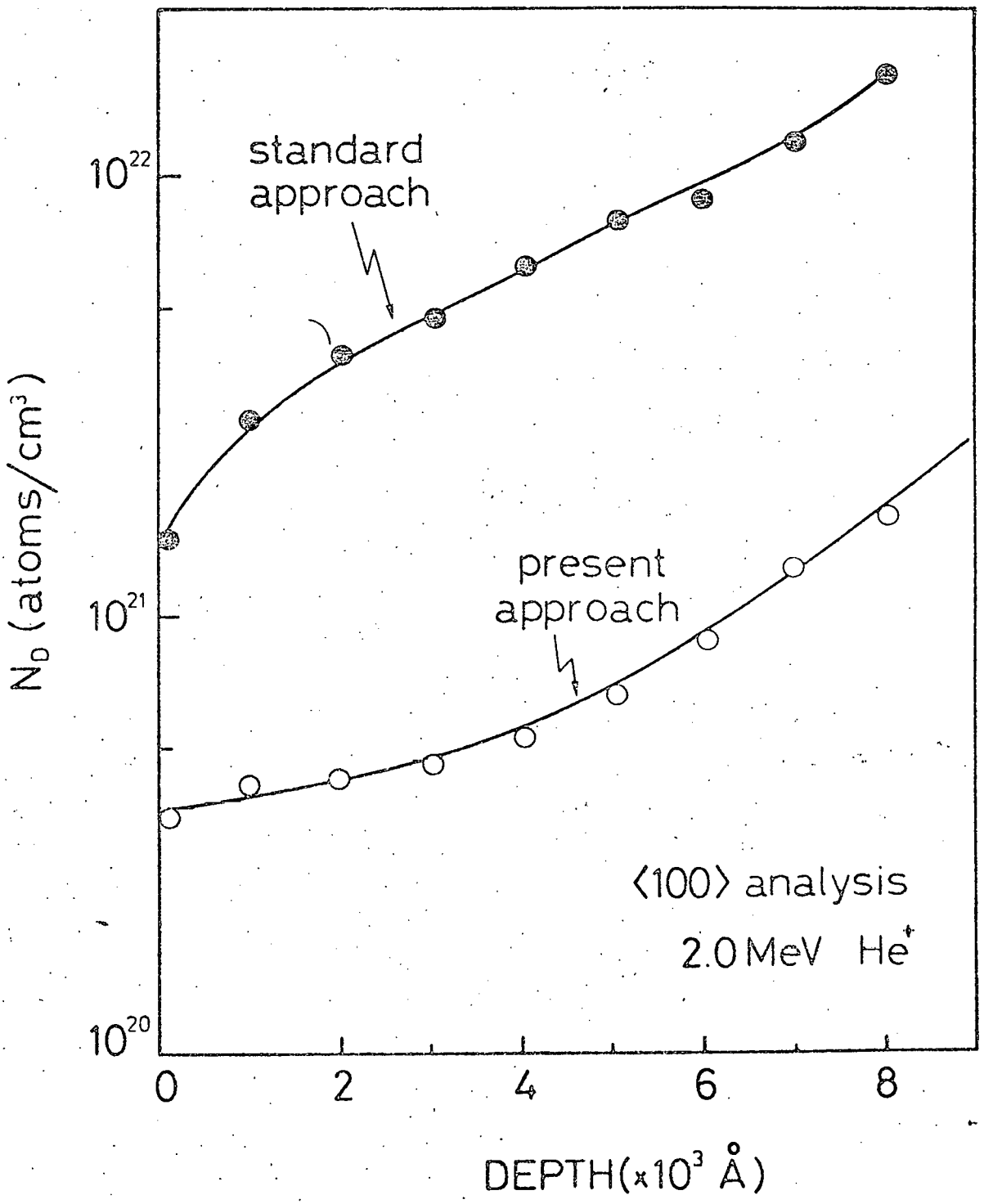
standard
approach
present
approach
10^{22}
10^{21}
10^{20}
N_D (atoms/cm^3)
⟨100⟩ analysis
2.0 MeV He^+
0
2
4
6
8
DEPTH(×10^3 Å)

Fig 1D